THE JOURNAL OF PHYSICAL CHEMISTRY Letters

Letter

pubs.acs.org/JPCL

Combined Experimental and Theoretical Approach to the Kinetics of Magnetite Crystal Growth from Primary Particles

Marc Widdrat, Emanuel Schneck, Victoria Reichel, Jens Baumgartner, Luca Bertinetti, Wouter Habraken, Klaas Bente, Peter Fratzl, and Damien Faivre*

Department of Biomaterials, Max Planck Institute of Colloids and Interfaces, Science Park Golm, 14424 Potsdam, Germany

Supporting Information

ABSTRACT: It is now recognized that nucleation and growth of crystals can occur not only by the addition of solvated ions but also by accretion of nanoparticles, in a process called nonclassical crystallization. The theoretical framework of such processes has only started to be described, partly due to the lack of kinetic or thermodynamic data. Here, we study the growth of magnetite nanoparticles from primary particles—nanometer-sized amorphous iron-rich precursors—in aqueous solution at different temperatures. We propose a theoretical framework to describe the growth of the nanoparticles and model both a diffusion-limited and a reaction-limited pathway to determine which of these best describes the rate-limiting step of the process. We show that, based on the measured iron concentration and the related calculated concentration of primary particles at the steady state, magnetite growth is likely a reaction-limited process, and within the framework of our model, we propose a phase diagram to summarize the observations.

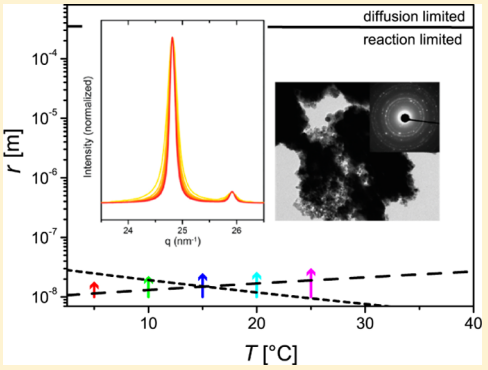

Crystallization is a fundamental process, which plays a key role in both natural and artificial phenomena. Natural examples encompass, for example, mineral formation in geological settings,[1] snowflakes,[2] or biomineral formation by organisms.[3,4] In turn and just to name a few, synthetic processes of crystallization range from single-crystal breeding[5] to materials production for electronics[6] or thin films.[7] Processes behind crystal nucleation and growth have been investigated experimentally[8,9] as well as theoretically.[10−12] However, the exact mechanisms associated with crystallization have often remained unclear, specifically in the case of aqueous processes. The classical nucleation theory[13] considers crystals being formed from single ions or molecules and was successfully utilized to describe crystallization for many years. Recent studies showed, however, strong evidence for alternative, so-called nonclassical nucleation routes.[14] These include the aggregation of ion-association complexes (calcium phosphate[15]), clusters (calcium carbonate[16]), or primary particles (PPs) (iron oxides[17]). The theoretical framework in which such processes take place has started to emerge.[18,19] For example, classical nucleation theory has been amended to take into account the presence of this nanoparticulate matter in the prenucleation stage of magnetite formation.[17]

Magnetite is a ubiquitous naturally occurring mineral with unique magnetic properties. It was shown by cryogenic transmission electron microscopy imaging (cryo-TEM) that it forms from PPs, which aggregate and subsequently nucleate.[17] It was also suggested that the crystal growth is PP-mediated and that despite the involvement of PPs, it follows the predictions of the classical theories, and in particular, a reaction-limited mechanism was proposed.[17] However, experimental data are lacking for a quantitative description of the pathway.[20] Here, we thus present a study of magnetite nanoparticle growth at different temperatures to determine the growth rates and the rate-limiting step.

In our assay, magnetite was formed by the addition of an iron solution in a reactor kept at constant pH by the concomitant addition of a NaOH solution (see the experimental details in the Supporting Information (SI) for details).[21,22] The reactor was kept at constant temperature. Magnetite crystal growth was investigated at five different temperatures (5, 10, 15, 20, and 25 °C), and each synthesis was reproduced in quadruplicate. X-ray diffraction patterns show typical magnetite peaks at every time point (Figure 1a), and a closer view of the 311 peak reveals its continuous narrowing (Figure 1b). The mean particle diameter was calculated from the Scherrer equation,[23] and particle growth was observed over time, as shown in Figure 1c. Transmission electron microscopy shows typical, highly aggregated magnetite nanoparticles (Figure 1d).

Particle growth over time is observed for all temperatures (Figure 2; see the SI for the full data set). After 8 h, larger particles are obtained at higher temperatures (compare purple points at 25 °C with red points obtained at 5 °C). In the experimental scenario stemming from our earlier cryo-EM observations,[17] the concentration of the PPs ([PP]) is time-dependent during the first minutes of the reaction prior to

Received: December 19, 2016
Accepted: February 22, 2017
Published: February 22, 2017

DOI: 10.1021/acs.jpclett.6b02977
J. Phys. Chem. Lett. 2017, 8, 1132−1136

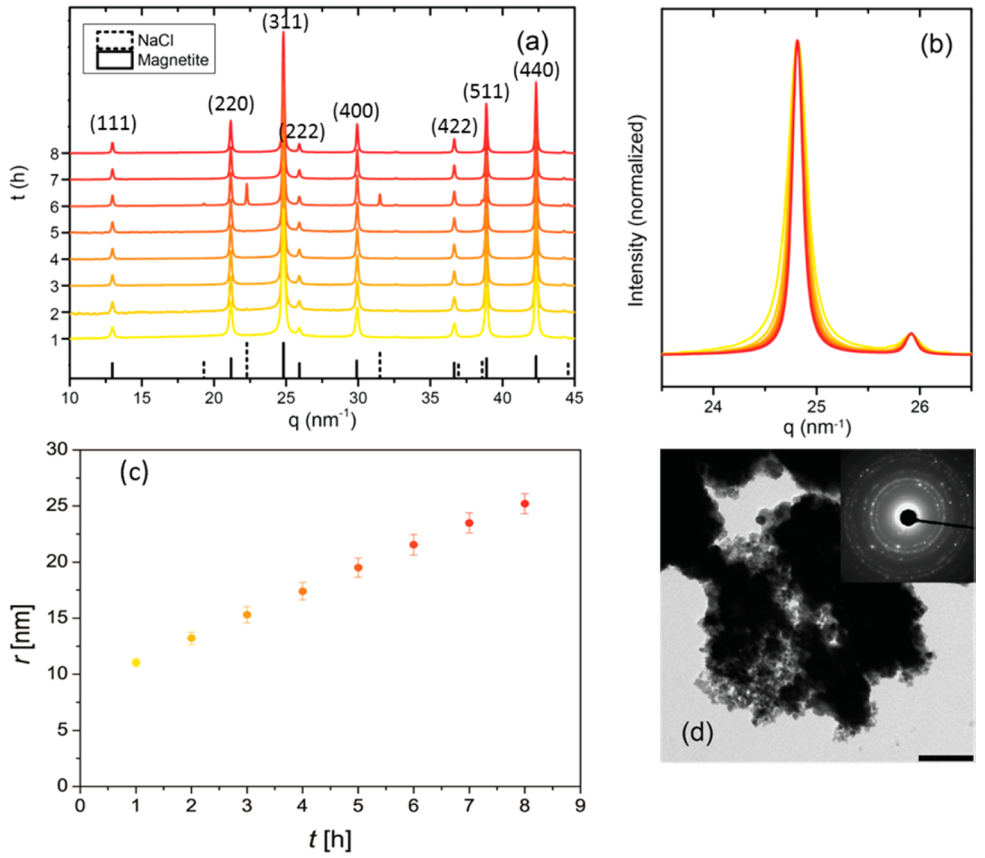

Figure 1. Summary of experimental results representative for all samples. (a) The XRD diagram shows a typical magnetite pattern at every time point (black solid lines). NaCl (black dotted lines) is sometimes observed besides magnetite. The chronological evolution is indicated by a color scale from yellow (early state) to red (late state), with the magnetite peaks indexed. (b) The insight into the 311 peak reveals the decrease of the full width at half-maximum. (c) Radius of the nanoparticles (r) with standard error as a function of time determined by averaging data for all syntheses at 15 °C. (d) TEM image of one representative sample (scale bar: 200 nm) showing highly aggregated nanoparticles of magnetite (inset: SAED pattern with magnetite rings).

magnetite nucleation. Then, [PP] reaches a steady-state where growth of the initially nucleated particles of size r_{init} takes over nucleation of new particles. Here, we first measure the particle size after 1 h and therefore already are in the steady-state regime.

The evolution of the particle size was modeled using the different scenarios qualitatively discussed above in order to extract more quantitative insights. The model assumes that the PPs (radius r_0 = 1 nm,[17] constant bulk concentration c_0) are homogeneously distributed within the medium, which is justified as the solutions were kept under continuous stirring, and bind to the growing magnetite particles with frequency c_0k. Here, k is a rate as specified below that may depend on the temperature and the radius r of the growing particles. Each binding event increases the volume V of a growing particle by an increment $V_0 = 4\pi r_0^3/3$, corresponding to the volume of a PP, so that $dV/dt = V_0c_0k$. For isotropic growth of the forming particles, as expected for a mineral crystallizing in a cubic system, we have $dV = 4\pi r^2\, dr$ and obtain a nonlinear differential equation for the evolution of the particle radius

$$\frac{dr}{dt} = \frac{V_0c_0k(r, T)}{4\pi r^2} \tag{1}$$

For the rate k, we consider two mechanisms, diffusion-limited ($k = k_{diff}$) and reaction-limited ($k = k_{reac}$) growth. We further assume that the magnetite particles grow from an initial particle with a radius r_{init}. For the diffusion-limited case, the Smoluchowsky description is used[24]

$$k_{diff} = 4\pi(r + r_0)(D + D_0) \tag{2}$$

Note that in this treatment neither the extension of the PPs nor the diffusion of the initially formed magnetite nanoparticles is neglected. The diffusion coefficients are represented with the common Stokes−Einstein result involving the temperature-dependent solution viscosity η

$$D = \frac{k_BT}{6\pi\eta r} \quad \text{and} \quad D_0 = \frac{k_BT}{6\pi\eta r_0} \tag{3}$$

For η, we used the tabulated values of water at 5, 10, 15, 20, and 25 °C.[25] For the reaction-limited case, we set the reactive area equal to the surface of a particle with the effective radius for the two-particle interaction ($r + r_0$), in analogy with eq 2, and we employ a simple Arrhenius factor[26] in order to account for an activation energy barrier ΔU

$$k_{reac} = 4\pi(r + r_0)^2k_0e^{-\Delta U/(k_BT)} \tag{4}$$

Here, k_0 is a temperature-independent pre-exponential factor reflecting both a finite reaction attempt frequency f_0 and the effect of an entropic contribution to the reaction free energy barrier ΔS, $k_0 = f_0e^{\Delta S/k_B}$.[27] It should be noted that in eq 1 the growth of the magnetite particles is assumed to be proportional to the concentration c_0 of the PP, that is, it is assumed that all

DOI: 10.1021/acs.jpclett.6b02977
J. Phys. Chem. Lett. 2017, 8, 1132−1136

PPs adsorb and react independently. Equation 1 thus does not explicitly account for crowding effects relevant in the reaction-limited case for high c_0. In practice, however, when using eq 1 in combination with eq 4, such crowding effects would merely manifest in a reduced numerical value of k_0.

The experimental data on the particle radii obtained at the different temperatures were modeled simultaneously based on common sets of model parameters. The free parameter r_{init} was common to all temperatures because it did not exhibit any significant temperature dependence (see the SI). In the diffusion-limited scenario, the adjustable parameters were c_0 and r_{init}. In the reaction-limited scenario ΔU, a prefactor $A = c_0 k_0$ and r_{init} were adjustable. Equation 1 was solved numerically, and the parameters were adjusted in a least-squares fit to achieve the best agreement, that is, with minimal χ^2 deviation between experimental and modeled values of $r(t)$ for the five different temperatures. The best-matching model parameters and the corresponding reduced χ^2 values are summarized in Table 1.

Table 1. Parameters of Diffusion-Limited and Reaction-Limited Models of the Evolution of the Particle Radius

model	χ_{red}^2	c_0 (m^{-3})	ΔU (kJ mol^{-1})	k_0 (s^{-1})	r_{init} (nm)
diffusion-limited	2.9	1.3×10^{16}[a]			7.2
reaction-limited	3.2		24	0.002[b]	9.4

[a]The experimental value is $c_0 = 2.3 \times 10^{20}$ m^{-3} assuming PPs with magnetite stoichiometry. [b]Using $c_0 = 2.3 \times 10^{20}$ m^{-3}.

In the diffusion-limited case (Figure 2a), the splitting of the theoretical curves for different temperatures is due to the temperature dependence of the diffusion coefficients (eq 3) involving the temperature-dependent solution viscosity. In the activation-limited case (Figure 2b), the splitting is linked to the height of the activation barrier ΔU (eq 4). It is seen that our experimental data are reproduced reasonably well by both the diffusion-limited model and the reaction-limited model, although the diffusion-limited model under-represents the temperature dependence. Even if, for example, the 5 °C curve presented a poorer match, we restrained our analysis here to the global data set and to the two main processes typically envisaged for such a process to get first hints toward a mechanistic picture. The obtained best-matching initial radii (Table 1; 7.2 nm for diffusion-limited and 9.4 nm for reaction-limited) are slightly larger than but comparable to those of the smallest magnetite particles found in earlier experiments (5 nm[17]). The reduced χ^2 deviation is similar for diffusion-limited ($\chi_{red}^2 \approx 2.9$) and reaction-limited scenarios ($\chi_{red}^2 \approx 3.2$) (Table 1). Therefore, without measurement of an additional experimental parameter, the modeling is also not able to decipher the origin of the process.

One such crucial parameter is the concentration of the PPs. It indeed appears as a fitting parameter in the diffusion-limited model and is concomitantly experimentally accessible. We thus determined the PP concentration via the iron amount as measured by ICP-OES. To this end, we considered as in the model only three iron-based components: the ions, the PPs, and the magnetite nanoparticles. Due to the very low solubility of iron in water, there is less than 1% iron left in the solution in the form of ions already from pH 4.[20] Therefore, virtually all iron is contained in PPs or larger magnetite nanoparticles. We magnetically separated the magnetite nanoparticles from the solution using a 100 mT magnet. The gradient produced by such a magnet attracts the magnetite nanoparticles within few minutes, whereas days would be necessary for the PPs to be removed (see the SI for full calculations). The measured iron concentration therefore originates from the PPs only. Assuming that the PPs are "proto-magnetite" following the results obtained on calcium carbonate system,[28] we obtained $c_0 \approx 2.3 \times 10^{20}$ m^{-3} (see the SI for full calculations). If we however choose a ferrihydrite model based on earlier considerations[17] and use a dedicated model for hypothetical ferrihydrite spherical particles[20] with crystallographic data from Michel et al.,[29] a similar order of magnitude is obtained ($c_0 \approx 15 \times 10^{20}$ m^{-3}). As an outcome of the modeled diffusion-limited scenario, an at least 4 orders of magnitude lower value of c_0 is obtained (Table 1). Therefore, the growth of magnetite is almost certainly not diffusion-limited but lies instead in the reaction-limited regime. Therefore, a free-energy barrier to PP adsorption is required, which we found to be as low as 24 kJ × mol^{-1} (Table 1). For activation-limited crystal growth, an activation energy between 40 and 80 kJ mol^{-1} is expected in the case of a process based on the addition of ions.[5] Alternatively, in a system involving poorly soluble species, oriented attachment of ZnS via nanoparticles leads to activation energies in the range of 125 kJ × mol^{-1}.[30] In this case, the activation energy for this surface activation-limited process becomes energetically more demanding because of the large number of atoms being integrated into the crystal surface simultaneously.

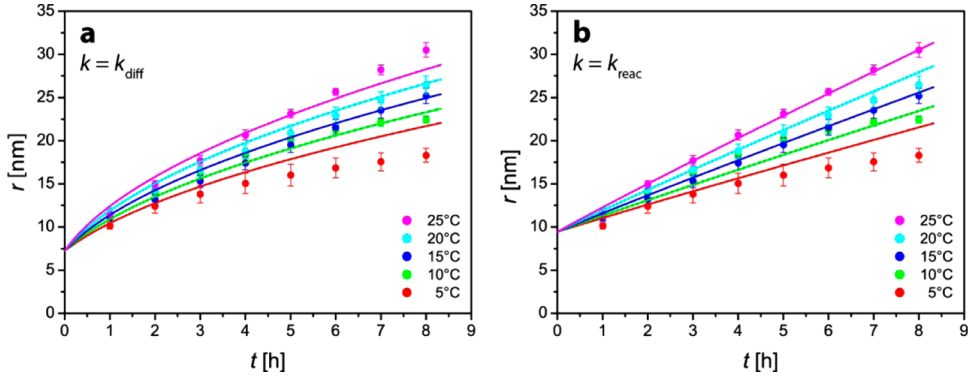

Figure 2. Evolution of the particle radius as obtained experimentally for various temperatures (symbols with standard errors) and as predicted by two different models for particle growth with adjustable model parameters (solid lines). (a) Diffusion-limited growth. (b) Reaction-limited growth.

DOI: 10.1021/acs.jpclett.6b02977
J. Phys. Chem. Lett. 2017, 8, 1132−1136

Using the most conservative experimental estimate of c_0 (c_0 = 2.3 × 10^{20} m^{-3} for PPs with magnetite stoichiometry), the reaction-limited model yields an estimate of the pre-exponential factor, $k_0 \approx 0.002$ s^{-1}, and, together with ΔU and r_{init}, a comprehensive description of the particle growth process and its temperature dependence.

As pointed out above, the described growth of the magnetite particles by adsorption of PPs takes place in the reaction-limited regime, that is, $k_{reac} \ll k_{diff}$ even though the energy barrier of the rate-limiting reaction is low. We note, however, that k_{diff} and k_{reac} have different dependence on the temperature T and on the particle radius r (see eqs 2−4). In other words, the growth at different temperatures and up to larger sizes may take place in a different regime. In order to illustrate this point, we show in Figure 3 a T−r phase diagram in which the solid line demarks the transition between diffusion-limited and reaction-limited growth, that is, when $k_{reac}(T,r) = k_{diff}(T,r)$. Arrows indicate the radius ranges covered in the growth experiments at the different temperatures. For the determination of the phase boundary, the experimental T dependence of η was described with a purely empirical continuous function. We obtain the critical particle radius for diffusion-limited growth in the range of several tens of micrometers (continuous line in Figure 3). Interestingly, its T dependence is weak. This behavior reflects that ΔU is numerically close to the equivalent energy barrier of water diffusion, ΔU_{diff}^{equiv} = 2.9 × 10^{-20} J,[31] which corresponds to the T dependence of the water diffusivity in a diffusion-limited scenario. In fact, this explains why the diffusion-limited scenario also qualitatively describes the experimental data points in Figure 2a. The phase diagram is however also important to predict alternative scenarios. For example, a significant T dependence of the critical radius is observed when ΔU is significantly larger or respectively smaller than ΔU_{diff}^{equiv} (Figure 3). For illustration, both cases shown ($\Delta U = 0.1\Delta U_{diff}^{equiv}$ and $\Delta U = 3\Delta U_{diff}^{equiv}$) were modeled with k_0 chosen such that the transition lines cross the range of temperatures and radii relevant for the present experimental data. It is seen that under certain circumstances, in terms of ΔU and k_0, the particle growth may start in the reaction-limited regime and end up limited by diffusion. Alternatively, growth at low temperatures may be reaction-limited, while growth at higher temperatures is diffusion-limited, or vice versa.

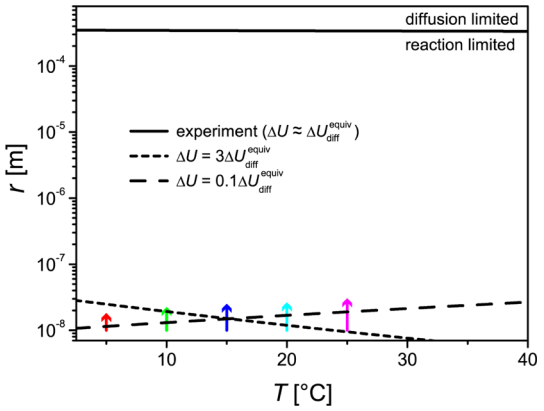

Figure 3. Radius−temperature phase diagram for the particle growth mechanism. Arrows indicate the radius ranges covered in the growth experiments at the different temperatures. The solid line demarks the transition between diffusion-limited and reaction-limited growth, that is, when $k_{reac}(T,r) = k_{diff}(T,r)$ for the experimentally obtained energy barrier ΔU. Dashed lines indicate the predicted phase boundaries when assuming lower or higher values of ΔU.

Particle growth in general can also be affected also by other mechanisms than those used in our simple model, either related to particle nucleation during the reaction, particle fusion, or collision-induced breakage or aggregation under highly turbulent conditions.[32] However, in view of the robustness of the model parameters with respect to particle size polydispersity (Figure S6) representing continuous magnetite particle nucleation and because of the mild reaction conditions applied here (Reynolds numbers typical of laminar flows), those mechanisms were not taken into account.

In summary, we have quantified the influence of the temperature on magnetite formation via the coprecipitation method in solution. We modeled different scenarios, which led us to propose that the main rate-determining step for the growth of magnetite nanoparticles is a reaction-limited process where PPs need to bind to the surface of the growing magnetite particles. The presented phase diagram enables discussion of scenarios where both regimes can be present or alternatively may take over. We are convinced that this integrated approach will lead to a better understanding of the complicated nucleation and growth processes found out recently.

■ ASSOCIATED CONTENT

Supporting Information

The Supporting Information is available free of charge on the ACS Publications website at DOI: 10.1021/acs.jpclett.6b02977.

Materials and methods details, full data set, and additional discussion (PDF)

■ AUTHOR INFORMATION

Corresponding Author

*E-mail: damien.faivre@mpikg.mpg.de.

ORCID

Damien Faivre: 0000-0001-6191-3389

Notes

The authors declare no competing financial interest.

■ ACKNOWLEDGMENTS

This work was supported by the Max Planck society, the European Union (Project Bio2MaN4MRI n°245542), the European Research Council (Starting Grant MB2 n°256915), and the German Research Foundation (DFG) (Emmy-Noether grant (SCHN 1396/1) and ERA-CHEM (FA835/12-1)). We thank Jeannette Steffen for elemental concentration measurements and Prof. Carl Krill (U. Ulm) for discussions.

■ REFERENCES

(1) Tapponnier, P.; Zhiqin, X.; Roger, F.; Meyer, B.; Arnaud, N.; Wittlinger, G.; Jingsui, Y. Oblique stepwise rise and growth of the tibet plateau. *Science* **2001**, *294*, 1671−1677.

(2) Manton, M. J. The physics of clouds in the atmosphere. *Rep. Prog. Phys.* **1983**, *46*, 1393−1444.

(3) Fratzl, P.; Weinkamer, R. Nature's hierarchical materials. *Prog. Mater. Sci.* **2007**, *52*, 1263−1334.

(4) Faivre, D.; Godec, T. U. From bacteria to mollusks: The principles underlying the biomineralization of iron oxide materials. *Angew. Chem., Int. Ed.* **2015**, *54*, 4728−4747.

(5) Mullin *Crystallization*. 4th ed.; Butterworth Heinemann: Oxford, 2001; p 294.

(6) Sadoh, T.; Park, J. H.; Kurosawa, M.; Miyao, M. Low-temperature metal-induced crystallization of orientation-controlled sige on insulator

DOI: 10.1021/acs.jpclett.6b02977
J. Phys. Chem. Lett. 2017, 8, 1132−1136

for flexible electronics. In *Ulsi process integration 8*; Claeys, C., Tao, M., Murota, J., Iwai, H., Deleonibus, S., Eds.; Electrochemical Society Inc.: Pennington, NJ, 2013; Vol. *58*, pp 213−221.
(7) Alexe, M.; Ziese, M.; Hesse, D.; Esquinazi, P.; Yamauchi, K.; Fukushima, T.; Picozzi, S.; Gosele, U. Ferroelectric switching in multiferroic magnetite (fe3o4) thin films. *Adv. Mater.* **2009**, *21*, 4452−4455.
(8) Eberl, D. D.; Drits, V. A.; Srodon, J. Deducing growth mechanisms for minerals from the shapes of crystal size distributions. *Am. J. Sci.* **1998**, *298*, 499−533.
(9) Kile, D. E.; Eberl, D. D. On the origin of size-dependent and size-independent crystal growth: Influence of advection and diffusion. *Am. Mineral.* **2003**, *88*, 1514−1521.
(10) Binder, K. Theory of 1st-order phase-transitions. *Rep. Prog. Phys.* **1987**, *50*, 783−859.
(11) Cahn, J. W. Theory of crystal growth and interface motion in crystalline materials. *Acta Metall.* **1960**, *8*, 554−562.
(12) Fratzl, P.; Lebowitz, J. L.; Penrose, O.; Amar, J. Scaling functions, self-similarity, and the morphology of phase-separating systems. *Phys. Rev. B: Condens. Matter Mater. Phys.* **1991**, *44*, 4794−4811.
(13) Becker, R.; Doring, W. Kinetic treatment of germ formation in supersaturated vapour. *Ann. Phys.* **1935**, *416*, 719−752.
(14) De Yoreo, J. J.; Gilbert, P. U. P. A.; Sommerdijk, N. A. J. M.; Penn, R. L.; Whitelam, S.; Joester, D.; Zhang, H.; Rimer, J. D.; Navrotsky, A.; Banfield, J. F.; Wallace, A. F.; Michel, F. M.; Meldrum, F. C.; Cölfen, H.; Dove, P. M. Crystallization by particle attachment in synthetic, biogenic, and geologic environments. *Science* **2015**, *349*, aaa6760.
(15) Habraken, W.; Tao, J. H.; Brylka, L. J.; Friedrich, H.; Bertinetti, L.; Schenk, A. S.; Verch, A.; Dmitrovic, V.; Bomans, P. H. H.; Frederik, P. M.; Laven, J.; van der Schoot, P.; Aichmayer, B.; de With, G.; DeYoreo, J. J.; Sommerdijk, N. Ion-association complexes unite classical and non-classical theories for the biomimetic nucleation of calcium phosphate. *Nat. Commun.* **2013**, *4*, 1507.
(16) Gebauer, D.; Volkel, A.; Cölfen, H. Stable prenucleation calcium carbonate clusters. *Science* **2008**, *322*, 1819−1822.
(17) Baumgartner, J.; Dey, A.; Bomans, P. H. H.; Le Coadou, C.; Fratzl, P.; Sommerdijk, N. A. J. M.; Faivre, D. Nucleation and growth of magnetite from solution. *Nat. Mater.* **2013**, *12*, 310−314.
(18) Demichelis, R.; Raiteri, P.; Gale, J. D.; Quigley, D.; Gebauer, D. Stable prenucleation mineral clusters are liquid-like ionic polymers. *Nat. Commun.* **2011**, *2*, 590.
(19) Penn, R. L. Kinetics of oriented aggregation. *J. Phys. Chem. B* **2004**, *108*, 12707−12712.
(20) Baumgartner, J.; Faivre, D. Iron solubility, colloids and their impact on iron (oxyhydr)oxide formation from solution. *Earth-Sci. Rev.* **2015**, *150*, 520−530.
(21) Baumgartner, J.; Bertinetti, L.; Widdrat, M.; Hirt, A. M.; Faivre, D. Formation of magnetite nanoparticles at low temperature: From superparamagnetic to stable single domain particles. *PLoS One* **2013**, *8*, e57070.
(22) Widdrat, M.; Kumari, M.; Tompa, É.; Pósfai, M.; Hirt, A. M.; Faivre, D. Keeping nanoparticles fully functional: Long-term storage and alteration of magnetite. *ChemPlusChem* **2014**, *79*, 1225−1233.
(23) Patterson, A. L. The scherrer formula for x-ray particle size determination. *Phys. Rev.* **1939**, *56*, 978−982.
(24) Calef, D. F.; Deutch, J. M. Diffusion-controlled reactions. *Annu. Rev. Phys. Chem.* **1983**, *34*, 493−524.
(25) Kampmeyer, P. M. The temperature dependence of viscosity for water and mercury. *J. Appl. Phys.* **1952**, *23*, 99−102.
(26) Hanggi, P.; Talkner, P.; Borkovec, M. Reaction-rate theory - 50 years after kramers. *Rev. Mod. Phys.* **1990**, *62*, 251−341.
(27) Kowalik, B.; Schubert, T.; Wada, H.; Tanaka, M.; Netz, R. R.; Schneck, E. Combination of md simulations with two-state kinetic rate modeling elucidates the chain melting transition of phospholipid bilayers for different hydration levels. *J. Phys. Chem. B* **2015**, *119*, 14157−14167.
(28) Gebauer, D.; Gunawidjaja, P. N.; Ko, J. Y. P.; Bacsik, Z.; Aziz, B.; Liu, L. J.; Hu, Y. F.; Bergstrom, L.; Tai, C. W.; Sham, T. K.; Eden, M.; Hedin, N. Proto-calcite and proto-vaterite in amorphous calcium carbonates. *Angew. Chem., Int. Ed.* **2010**, *49*, 8889−8891.
(29) Michel, F. M.; Ehm, L.; Antao, S. M.; Lee, P. L.; Chupas, P. J.; Liu, G.; Strongin, D. R.; Schoonen, M. A. A.; Phillips, B. L.; Parise, J. B. The structure of ferrihydrite, a nanocrystalline material. *Science* **2007**, *316*, 1726−1729.
(30) Huang, F.; Zhang, H.; Banfield, J. F. Two-stage crystal-growth kinetics observed during hydrothermal coarsening of nanocrystalline zns. *Nano Lett.* **2003**, *3*, 373−378.
(31) Tanaka, K. Measurements of self-diffusion coefficients of water in pure water and in aqueous electrolyte solutions. *J. Chem. Soc., Faraday Trans. 1* **1975**, *71*, 1127−1131.
(32) Pohar, A.; Likozar, B. Dissolution, nucleation, crystal growth, crystal aggregation, and particle breakage of amlodipine salts: Modeling crystallization kinetics and thermodynamic equilibrium, scale-up, and optimization. *Ind. Eng. Chem. Res.* **2014**, *53*, 10762−10774.

DOI: 10.1021/acs.jpclett.6b02977
J. Phys. Chem. Lett. 2017, 8, 1132−1136